ISSN: 1410-8917
e-ISSN: 2597-9914

Jurnal Kimia Sains dan Aplikasi 26 (4) (2023): 133-142

Jurnal Kimia Sains dan Aplikasi
Journal of Scientific and Applied Chemistry

Journal homepage: http://ejournal.undip.ac.id/index.php/ksa

Study of Synthesis and Performance of Clay and Clay-Manganese Monoliths for Mercury Ion Removal from Water

Aula Chairunnisak *, Darmadi Darmadi, Adisalamun Adisalamun, Mukramah Yusuf, Syawaliah Mukhtar, Ulfa Rijal Safitri, Oppie Azza Shafira

Department of Chemical Engineering, Faculty of Engineering, Universitas Syiah Kuala, Aceh, Indonesia

* Corresponding author: aulachairunnisak@usk.ac.id

https://doi.org/10.14710/jksa.26.4.133-142

Article Info

Article history:

Received: 23rd March 2023
Revised: 02nd June 2023
Accepted: 11th June 2023
Online: 30th June 2023

Keywords:
mercury; adsorption; clay; manganese; monolith

Abstract

The pollution caused by mercury (Hg) is a matter of concern regarding worldwide ecosystems and public health. It is dangerous as it is highly poisonous and has more ways to get exposed than other heavy metal ions. Recently, the application of biomaterials with varying structures and designs for mercury adsorption has grown. In this research, clay monoliths (CM) and clay-manganese monoliths (CMM) were synthesized, investigated, and compared regarding their ability to adsorb mercury ions from water to determine the most effective adsorbents. CM and CMM were extruded through a stainless-steel molder with dimensions of 7 holes, 9 mm in radius, and 20 mm in height. The surface morphologies of both adsorbents were characterized using infrared (IR) spectroscopy and scanning electron microscopy (SEM). The effects of contact time (40, 80, 120, 160, 200, and 240 minutes) and initial concentrations (3–5 mg/L) were applied to evaluate both adsorption processes. The experiment was conducted in a batch reactor using a monolithic adsorbent that operated for 240 minutes. The experimental equilibrium data of the adsorption were examined with Langmuir and Freundlich models to find the best-fit isotherm. In the kinetic study, the pseudo-first-order was investigated in both linear and nonlinear models. The adsorption results showed that CMM had the highest adsorption efficiency (42.7%). The equilibrium study concluded that the Langmuir was the most significant isotherm model. The highest monolayer capacity and Langmuir constants (K_L and a_L) were 0.396, 1.329, and 0.396, respectively. The adsorption of both adsorbents was well displayed in the pseudo-first-order non-linear model. Experiments and processed data compromise the finding that CMM is more effective than CM at adsorbing mercury ions.

1. Introduction

Mercury is a non-biodegradable, highly hazardous metal originating mainly from geological and human contamination [1]. Due to mercury's high level of toxicity, it must be regarded as a pollutant even though its abundance in the environment is considered relatively low. According to the World Health Organization, mercury is one of ten substances of concern, and 0.002 mg/L was deemed the allowable level [2]. The human-caused environmental sources include metals like iron and steel industries [3], concrete industries [4, 5, 6], non-metallic metal producing [7], chloro-alkali industry [8], and on-site mercury manufacture industries [9]. Mercury could be transferred and circulated in water, soil, and air, resulting in significant pollution [1]. Mercury's resident frequency in the environment is between 0.8 and 1.7 years. In the study by Kern and Jones [10], the connection between mercury in human organs and its impact on Autism Spectrum Disorder (ASD) was investigated. A correlation between mercury exposure and infertility has been investigated. Researchers discovered that exposure to heavy metals such as mercury is one of the root causes of infertility [11] due to the body's intake of polluted fish and shellfish, cavities amalgams,

malfunctioning thermometers, fluorescent bulbs, phone batteries, and skin-and-body lightening care product [2].

In addition to the global regulation of mercury emissions, the remediation of mercury-contaminated water is an important goal that may reduce the harmful effects of mercury on individuals and ecosystems [12]. Numerous researchers have developed numerous techniques for removing mercury oxide from exhaust gases, including adsorption, catalyst oxidation, bio- oxidation, photocatalytic oxidation, plasma oxidation, photochemical, advanced oxidation, and simultaneous removal using Selective Catalytic Reduction (SCR) catalyst [13]. Adsorption has been the most frequent approach for remediating Hg-contaminated water. Developing low-cost, environmentally acceptable, and highly effective adsorbents is the key to its large- scale implementation [14]. In recent years, generating affordable yet reliable adsorbents has been essential in this sector. The researchers predicted that adsorption would be the most effective, competent, and widely utilized crucial technology in the water treatment process [15, 16, 17].

Clay is a fine crystalline particle made predominantly of alumina, silica, water-based, and covered rock [18]. For over a decade, clay, a fine-grained natural raw material, has been used as an excellent adsorbent for tracing heavy metal ions in an aqueous solution, gaining considerable interest. Clay exhibits flexibility across a varied range of water content and can become rigid when dry [19]. Clays were initially considered the most effective adsorbents because of their significant ion exchange capability, wide face area, excellent mechanical and chemical stability, and bilayer structure [20, 21]. Positive-charged ions on the outermost layer of clay indicate a larger tendency for binding negative-charged ions [22]. Clays and clay minerals are good adsorbent materials for eliminating harmful metal ions from water. Clays are preferred over commercially available adsorbents because of their low cost, wide availability, high specific surface area, excellent adsorption capabilities, non-toxic nature, and enormous capacity for ion exchange [23]. For this reason, a previous study has investigated using organic or synthetically modified clays as adsorbents for water treatment [24].

Metal oxides such as zinc oxides (ZnO), aluminum oxides (Al_2O_3), cerium oxides (CeO_2), and manganese oxides (MnO_2) have recently been widely exploited as extremely effective adsorbents for extracting heavy metal contaminants from sewage water [25, 26]. Because of its superior adsorption capability and good selectivity, MnO_2 is regarded as a viable choice for pollution removal. A potential loading approach was suggested using a mechanically reinforcing host material to load MnO_2 to overcome these crucial problems. This technique may provide an even distribution of MnO_2, efficiently remove it from the water solution, and boost its adsorption efficiency. A potential loading approach was suggested using physically reinforced site objects to support MnO_2 to solve these crucial problems. By using this method, MnO_2 could be distributed uniformly, separated efficiently from the aqueous solution, and its adsorption effectiveness could be further improved.

In order to remove mercury ions from aqueous solutions, the primary objective of this work is to construct an inexpensive, simple, and novel adsorbent proposed from clay and enriched with Mn oxides. In this work, activated pure clay and clay-enriched Mn were prepared in a more stable structure called monolith using a stainless-steel molder. The clay dough was prepared by some processes, such as mixing, molding, thermal consolidation, and drying. The constructed monoliths, CM and CMM, were investigated for their surface characteristics and performance in adsorbing mercury ions. The performance and behavior of CM and CMM were identified by efficiency adsorption, isotherm, and kinetic study. The specific objectives of this work are (1) to explore the physicochemical characteristics of the designed monoliths (CM and CMM), (2) to determine the removal capacity of mercury ion as the impact of initial concentrations and contact time on the adsorption CM and CMM adsorbents, and (3) to unravel the mercury ion removal mechanisms by CM and CMM adsorbent through isotherms and kinetics study. Applying natural and metal-modified adsorbents in a monolithic form in this work could assist in the purification and removal of hazardous metals from water and wastewater.

2. Materials and Methods

2.1. Materials

Raw clay was obtained from Sigli, Pidie District, Aceh Province, Indonesia. $Hg(NO_3)_2$ (Merck) was used as a mercury stock solution. In CMM modification, MnO_2 (Pudak Scientific) was applied as the doped in the mixture. CM and CMM dough was extruded through a molder with specifications of 9 mm in radius, 20 mm in height, and 7 honeycomb holes. These molds were designed in-house and manufactured through high- grade 316 stainless steel.

2.2. Synthesis of CM and CMM

Clay was diluted with distilled water for 5 minutes and then decanted repeatedly to eliminate contaminants. The slurry was sun-dried for two days to remove the surface water. The dried clay was ground using a ball mill, sifted through a 100-mesh sieve, and deposited in a vacuum-sealed container. This powdered clay was employed as a component of monolith adsorbent. The CM process combined powdered clay with distilled water to create a dough to be shaped and set. For the construction of the CMM, powdered clay was used with varying mass percentages of MnO_2 (0, 2, and 5% weight). Then, a sufficient amount of distillate water was added to this doped combination to produce a smooth and firm dough. The dough was extruded by a honeycomb molder with dimensions of 9 mm radius, 20 mm height, and 7 holes. The clay paste was dried in the open air for two days before being calcinated in a furnace (Furnace 51148, Nabertherm, Germany) at 600°C for 3 hours. Figure 1 shows the procedure of CM and CMM syntheses.

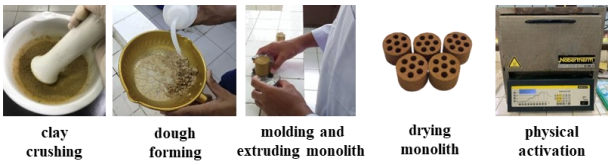

Figure 1. Schematic procedure of CM and CMM syntheses

2.3. Characterization of Adsorbents

The presence of functional groups in adsorbents was confirmed using a Fourier transform infrared spectrometer (SHIMADZU P-21) in the wavelength range of 4000 to 400 cm^{-1}. The adsorbents' surface form, structures, and elemental distribution were investigated using a scanning electron microscope (HITACHI TM 3000).

2.4. Adsorption Experiments

The Hg^{2+} solution was prepared by dissolving 1000 mg/L Hg^{2+} in a 3 to 5 mg/L concentration range. A single monolith was used in each adsorption batch with a total adsorbent mass of 2 grams. For the batch attempts, 2 grams of synthesized adsorbent and 250 mL of Hg^{2+} solution were added to a batch reactor for 240 minutes. During adsorption, the solution was agitated using a magnetic stirrer at 110 rpm. Ten mL of filtrate was collected every 40 minutes to analyze the concentration of Hg^{2+} using an Atomic Absorption Spectrophotometer (AAS). During the kinetic investigations, each adsorbent was put in a batch reactor containing Hg^{2+} solution with 3 and 5 mg/L initial concentrations. The filtrate was evaluated for the final Hg^{2+} content at various time intervals (0, 40, 80, 160, and 240 minutes). Various equations were employed to obtain comprehensive information regarding the adsorption process, such as efficiency, isotherm, and kinetic study. The equation for determining adsorption efficiency was calculated using the initial and final concentrations of Hg^{2+}, as indicated in Equation (1).

$$\text{Efficiency} = \frac{Co-Ct}{Co} \times 100\% \quad (1)$$

where, Co represents the starting concentration of the solution before adsorption (mg/L), and Ct represents the concentration of the solution after adsorption at a particular contact time (mg/L).

3. Results and Discussion

3.1. Characterization

Figure 2 and Table 1 display the Fourier-transform infrared spectra of calcined CM and CMM. At 3624 cm^{-1}, two different peaks in the spectra correspond to OH stretching vibrations originating from Al-Al-OH stresses [27]. The broad peak at 3434 cm^{-1} to 3400 cm^{-1} corresponds to the OH stretching of H-bonded water [28]. Si-O bonding vibration caused the bends at 1032 cm^{-1} and 797 cm^{-1}. The peak at 1032 cm^{-1} indicates a single bond of Si-O vibration. In contrast, the peak at 797 cm^{-1} indicates a double bond of quartz vibration. Furthermore, the aluminum bond is found at 538 cm^{-1}, ascribed to the deformation vibration of Al(IV)-OSi [29]. Bands from 400 cm^{-1} to 800 cm^{-1} were identified as Mn-O lattice vibration in the CMM. Three moderately strong IR bands are found at 427, 482, and 514 cm^{-1}, corresponding well to the IR characteristic bands of manganese oxides. The location and intensity of the distinctive adsorption bands are identical, showing that the IR characteristic bands of Mn-O vibrations are virtually completely independent of the synthesis processes [30].

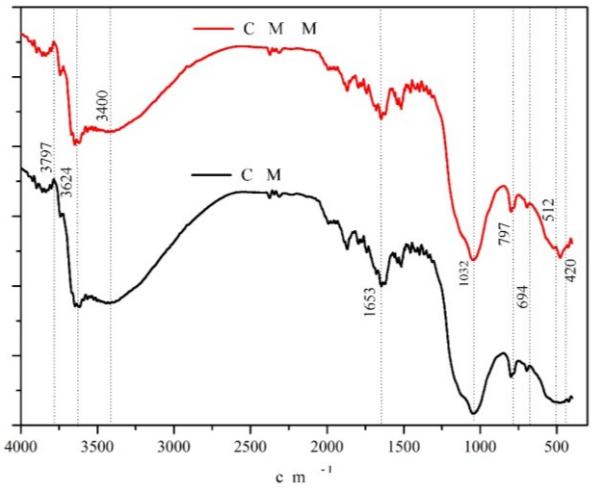

Figure 2. FTIR spectra of CM and CMM

Table 1. The principal IR bands and their corresponding species of CM and CMM

CM		CMM	
Wavenumber (cm^{-1})	Corresponding species	Wavenumber (cm^{-1})	Corresponding species
-		420	Mn-O
-	-	538	Al-O-Si
797	Si-O-Si	797	Si-O-Si
1032	Si-O	1032	Si-O
1653	H-O-H of water	1653	H-O-H of water
3434	OH of water	3434	OH of water
3624	Al-Al-OH	3624	Al-Al-OH

A 3000-magnification SEM is utilized to investigate the surface morphology of both adsorbents, as shown in Figures 2a and 2b. Figure 2a depicts the majority of the CM surface as flat and plate-like. This shape could refer to the montmorillonite structure in the clay. Previous research has shown that the clay monolith is made of particle agglomerates of different sizes and irregular shapes [31]. The surface pore of CMM changes after manganese oxide doping. The most notable changes were the pore structure and morphology of the improved adsorbent. Manganese coating tends to transform the clay surface into filament structures and sphere-like forms with small holes [32]. The sea urchin-like structure comprised several flakes emanating from its center. The flakes were very thin nanowall sheets with thicknesses ranging from three to ten nanometers. The pore size and site availability were the most significant distinctions between the visualizations in Figures 3a and 3b. Because CMM has wider pores than CM adsorbent, the manganese-doped modification successfully increased the adsorbent's availability and active site.

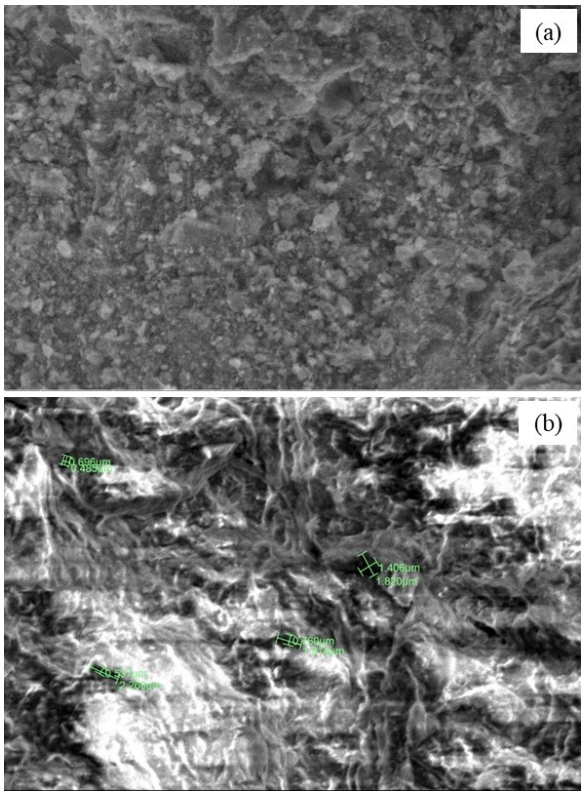

Figure 3. Scanning electron microscope morphologies of (a) CM and (b) CMM adsorbents with a 3000 times magnification

3.2. Effect of Contact Time on Adsorption Efficiency

The efficiency observed in this investigation was the proportion of Hg^{2+} metal ions adsorbed by clay adsorbents containing 0%, 2%, and 5% MnO_2 filler for contact times of 0, 40, 80, 120, 160, 200, and 240 minutes. Figure 4 illustrates the correlation between efficiency and contact time. The adsorption efficiency tends to improve significantly within the first 160 minutes hence the longer the contact time, the more engagements of Hg^{2+} metal ions that can adhere to the adsorbent's binding sites. Then, the efficiency improved gradually from 160 to 200 minutes and remained relatively stable or decreased slightly from 200 to 240 minutes. The efficiency of the 0% MnO_2-loaded CM (CM) declined from 29.9% to 28.8% at a solution concentration of 3 mg/L from 200 to 240 minutes (Figure 4a). 5% MNO_2-loaded CMM (CMM 5%) had the highest adsorption efficiency of 42.7%, followed by 2% MNO_2-loaded CMM (CMM 2%) of 34.0% and CM of 29.7% (Figure 4a). The doped or loaded form of MnO_2 is recognized for lowering the number of heavy metals in wastewater because of its relatively high surface area, microstructure, and OH functional groups, which can react with metals, phosphates, and other ions [33].

Adsorption efficiency can be reduced when the adsorbent desorbs. In Figure 4a, at a solution concentration of 3 mg/L from 200 to 240 minutes, the CM's efficacy decreased from 29.9% to 28.8%. This occurred as a result of adsorbent desorption. Desorption may occur because the adsorbent's surface is already saturated and in equilibrium, allowing the adsorbent to release the Hg^{2+} metal ions that were initially absorbed by the adsorbent [34]. When adsorption effectiveness decreases, the adsorbent is more likely to release than adhere to the adsorbate because the adsorbent has exceeded the maximum adsorption limit. The formation of van der Waals bonds occurred during the adsorption process. Because these bonds are very weak, the adsorbate that was previously bonded to the adsorbent can be readily dislodged from its hold (pores) [35].

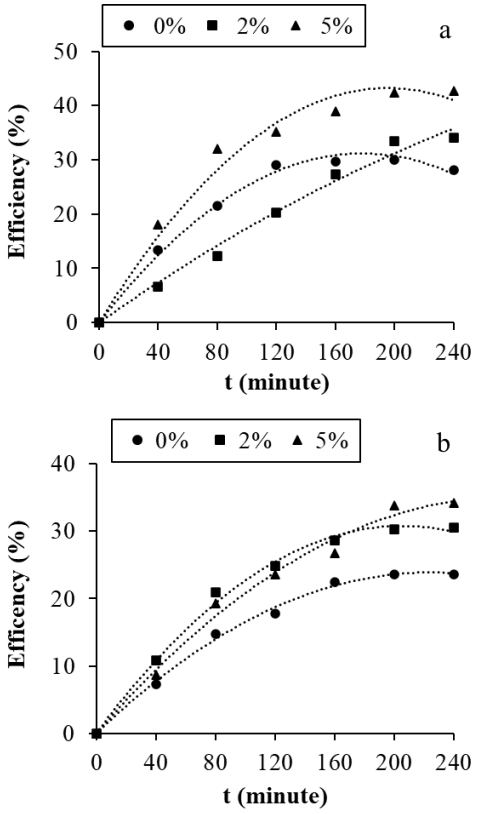

Figure 4. The correlation between operation time and efficiency at various initial concentrations (a) 3 mg/L and (b) 5 mg/L

According to the results, the sharp adsorption lasted 160 minutes and reached minor gaps in efficiency until it reached the equilibrium stage after 240 minutes. The binding ions with activated pores on the surface of CM and CMM were responsible for the remarkable efficiency. In this study, the desorption process of CM in 3 mg/L Hg^{2+} solution resulted in a slight reduction in adsorption efficiency from 29.9% to 28.8%. At low concentrations, the low binding ionic strength at the surface pores results in the adsorbate being released into the solution during the remaining contact time in the process.

3.3. Effect of Initial Adsorbate Concentration on Adsorption Efficiency

The effects of the initial concentration of the solution on the adsorption rate were explored by plotting a graph of the initial concentration versus the contact time, which is displayed in Figure 5. The adsorption capacity (qt) values of CM against Hg^{2+} were 0.058, 0.093, 0.125, 0.128, 0.129, and 0.121 mg/g at 3 mg/L, and 0.044, 0.089, 0.108, 0.135, 0.143, and 0.143 mg/g at 5 mg/L at contact times of 40, 80, 120, 160, 200, and 240 minutes, respectively. The adsorption capacity (qt) values of CMM 2% were 0.029, 0.053, 0.088, 0.118, 0.144, 0.146 mg/g at 3 mg/L, and 0.065, 0.126, 0.15, 0.173, 0.183, 0.184 mg/g at 5 mg/L

during contact times of 40, 80, 120, 160, 200, and 240 minutes. The adsorption capacity (qt) values of CMM 5% at initial solution concentrations (Co) of 3 and 5 mg/L obtained after 40, 80, 120, 160, 200, and 240 minutes in a row were 0.078, 0.138, 0.151, 0.168, 0.183, and 0.184 mg/g, and 0.053, 0.116, 0.143, 0.161, 0.204, and 206 mg/g. The adsorption capacity (qt) develops with the contact time, indicating that the adsorbent's adsorption rate of Hg^{2+} tends to increase. This is because the adsorbent pores are still devoid of adsorbate particles at the beginning of the adsorption process, and the potential for adsorbate particles to be adsorbed on the adsorbent pores is still fairly considerable, resulting in a significant shift in adsorption capacity [36].

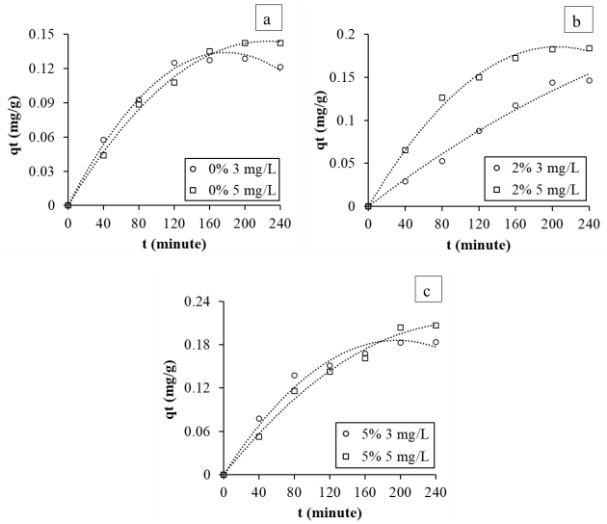

Figure 5. Effect of initial concentration on the adsorption capacity for Hg^{2+} using (a) CM, (b) CMM 2%, and (c) CMM 5%

The increase in adsorption capacity correlates to an increase in adsorbate concentration. Due to the high initial concentration, more of the Hg^{2+} ions engage and collide with the adsorbent, increasing its adsorption capacity [37]. Figure 4(c) also demonstrates that the adsorption capacity at an initial concentration of 5 mg/L of adsorbate is greater than that at 3 mg/L. Adsorption capacity rises slightly to an increase in the number of Hg^{2+} ions bound to the active sites of the adsorbent, resulting in some adsorbed Hg^{2+} ions being proportional to the number of accessible adsorbent binding sites. The maximum adsorption capacity of Hg^{2+} ions of 0.206 mg/g was achieved by CMM 5% in 240 minutes with an initial concentration of 5 mg/L. Compared to the previous study, this efficiency is lower than its best capacity of 0.83 mg/g with an initial concentration of 2 mg/L [38]. This is because the structure of the monolith is different. There were 40 holes and thinner channel walls in prior work, whereas the monoliths here featured 7 holes and thicker hole spacing. A monolith with more holes and a narrower space offered a better adsorption process because mass transfer at a specific distance becomes shorter and has more collision possibilities in the surface area [39]. Table 2 presents the maximum adsorption capacity in this current work and several different adsorbents in removing Hg^{2+} ions.

Table 1. The adsorption capacities of different adsorbents for Hg^{2+} ions

Adsorbent material	Maximum adsorption capacity (mg/g)	Reference
Clay manganese monolith	0.206	current work
Zeolite-clay based monoliths	0.167	[38]
Functionalized activated carbon	85.6	[40]
Activated carbon-based rice husk	55.87	[41]
Magnetic bentonite	26.18	[42]
Chitosan-coated diatomite	116.2	[43]
Derived date pits	7.8	[44]
Mandarin peel with chemically modified	34.84	[45]
Synthesized zeolite Linde Type A from coal fly ash	0.44	[46]
Ion-imprinted polymer monoliths	0.005	[47]

3.4. Adsorption Isotherm

The adsorption isotherm determines the relations between the adsorbate solution and the adsorbent and the adsorbent's maximum performance. Adsorption isotherms are the results of static adsorption experiments in which the adsorption process is performed in a container for a set time until equilibrium is attained [48]. The Langmuir and Freundlich adsorption isotherms were investigated in this work. The non-linear technique is employed in isotherm computations because it is more suited for isothermal equilibrium research. It has the advantage of not changing the error distribution as easily as the linear method [49]. The Langmuir model is represented in Equation (2) [50].

$$q_e = \frac{KL.Ce}{1+aL.C_e} \quad (2)$$

where q_e is the adsorption capacity of Hg (mg/g), C_e is the equilibrium concentration of Hg (mg/L), K_L (L/mg) and a_L (L/g) are the Langmuir coefficients.

The Freundlich model is followed in Equation 3 [50].

$$q_e = K_f . C_e^{1/n} \quad (3)$$

where q_e is the adsorption capacity of Hg (mg/g), C_e is the equilibrium concentration of Hg (mg/L), K_f is the calculated capacity in the Freundlich model (mg/g), and n is the intensity of the reaction.

The solver add-in tool in Microsoft® Excel was used in the calculation to estimate and optimize the isotherm parameters of non-linear equations. The best isotherm model was determined by identifying the lowest SSE (Sum of Square Error) value among the models. SSE was implicated as the value of the minimal objective function to result in the best isotherm parameters and to

minimalize the difference between theoretical and experimental data [51].

$$SSE = \sum_{i=1}^{n}\left(q_{e,exp} - q_{e,model}\right)_i^2 = 0 \quad (4)$$

Table 2 summarizes the optimization findings of the isotherm study in this work. The Langmuir isotherm model CMM 2% has a monolayer maximum adsorption capacity (Q_o) of 0.396 mg/g. CMM 5% has the greatest Langmuir constant values (K_L and a_L) of 0.336 L/g and 1.329 L/mg. According to the Freundlich isotherm model, CMM 5% exhibits a maximum adsorption capacity of 0.156 mg/g. The optimal isotherm model for each adsorbent has the lowest SSE [50]. As a result, it is apparent in Table 1 that the clay adsorbents with 0%, 2%, and 5% MnO_2 all match the Langmuir isotherm model. The Langmuir isotherm presupposes that adsorption happens on the adsorbent surface and that the active sites on the surface are homogeneous and finite. The adsorption process occurs in a single layer (monolayer) on the adsorbent surface, which is composed of homogeneous active sites, i.e., identical and energy-equivalent active sites, where the adsorbent can only adsorb one Hg^{2+} metal ion per active site with a uniform binding energy and no interactions between adjacently deposited Hg^{2+} ions [52].

Table 2. Summary of thermodynamic equilibrium isotherm data

Adsorbent	Langmuir isotherm				Freundlich isotherm		
	K_L (L/g)	a_L (L/mg)	Q_o (K_L/a_L)	SSE	K_f (mg/g)	N	SSE
CM	0.108	0.482	0.223	4.02×10^{-7}	0.084	2.441	1.11×10^{-6}
CMM 2%	0.102	0.257	0.396	3.17×10^{-7}	0.090	1.705	3.2×10^{-7}
CMM 5%	0.336	1.329	0.253	7.84×10^{-6}	0.156	4.248	9.89×10^{-6}

Based on the Langmuir isotherm's characteristics, several criteria will be considered to choose the adsorbent that will be the most effective and successful in adsorbing Hg^{2+} ions. The CMM 2% demonstrated the highest monolayer maximum adsorption capacity (Q_o). In comparison, the CMM 5% demonstrated the highest value for the Langmuir constant (K_L and a_L). The Langmuir constant (K_L) is a parameter in the Langmuir isotherm that describes the adsorption affinity of a material or adsorbent. Affinity is a key factor to consider when determining the efficacy of adsorption on pollutant targets; in fact, its function is more significant than that of the maximal monolayer [53]. In this investigation, adsorption was conducted in a mercury solution containing a relatively low concentration, making affinity a crucial variable. A high adsorption affinity value indicates an improvement in adsorption efficiency as the binding energy between the adsorbate and the adsorbent grows stronger and more adsorbate is deposited.

3.5. Kinetics Study

Adsorption kinetics is defined as the adsorption rate of the adsorbate due to its residence time on the surface of the adsorbent. The first-order pseudo Lagergren rate equation and the second-order H_o pseudo equation were utilized to determine the kinetic rate and mechanism of Hg^{2+} ions adsorption on the adsorbent [54]. A regression analysis based on linear and non-linear approaches was performed on these two equations to determine which model is more appropriate. The linear technique is evaluated based on the compatibility of the equation with experimental data. However, the non-linear method is evaluated based on the data optimization process and provides a more flexible fit function curve, hence minimizing the error value [55]. In order to find the most appropriate adsorption kinetics model, the regression coefficient (R^2) of linear and non-linear models must be compared [56]. The kinetic study equations in the present study are mentioned in Equations 5 to 8 [54]. The linear equation of pseudo-first-order is expressed in Equation (5).

$$ln(q_e - q_t) = ln(q_e) - k_1 t \quad (5)$$

where k_1 is the constant of pseudo-first-order (min^{-1}), which is obtained by plotting $\ln(q_e-q_t)$ vs. t, q_t is adsorption capacity in a certain time (mg/g), and t is operation time (minute).

The non-linear equation of pseudo-first-order is expressed in Equation (6).

$$q_t = q_e(1 - exp(-k_1 t)) \quad (6)$$

The linear equation of pseudo-second-order is expressed in Equation (7).

$$\frac{t}{q_t} = \frac{1}{k_2 q_e^2} + \frac{t}{q_e} \quad (7)$$

where k_2 is the constant of pseudo-second-order (g min/mg), obtained by plotting t/qt vs. t.

The non-linear equation of pseudo-second-order is expressed in Equation (8).

$$q_t = \frac{q_e^2 k_2 t}{1+q_e k_2 t} \quad (8)$$

Table 3 displays the outcomes of processing the adsorption kinetics data. The pseudo-first-order non- linear adsorption kinetics model was followed by all three adsorbents: CM, CMM 2%, and CMM 5%. At a solution concentration of 3 mg/L, the pseudo-first-order adsorption rate constants (k_1) of CM, CMM 2%, and CMM 5% were 0.0161, 0.0022, and 0.0141 min^{-1}, respectively. At a solution concentration of 5 mg/L, the pseudo-first-order adsorption rate constants (k_1) were 0.0090, 0.0114, and 0.0063 min^{-1}. The theoretical adsorption capacity ($q_{e\,cal}$) derived from the pseudo-first-order kinetic model aligned with the experimental adsorption capacity ($q_{e\,exp}$). According to a pseudo-first-order kinetic model, the adsorption rate of adsorbate ions is directly proportional to the number of free active sites on the surface of the adsorbent. The adsorption driving force (q_e-q_t) is directly related to the number of active sites; the more free active sites accessible, the higher the adsorption driving force. The pseudo-first-order model assumes that the adsorbate molecule will attach to a single active site on the surface of the adsorbent and that the adsorption process will take place physically (physical adsorption)

[57]. In addition, the pseudo-first-order kinetic model is more favorable for the adsorption process in low-concentration solutions [58], corresponding to the relatively low adsorbate concentrations in this investigation at 3 and 5 mg/L.

Table 3. The adsorption kinetic data of CM and CMM

C_o	Adsorbent	Parameter	Pseudo-first-order		Pseudo-second-order	
			Linear	non-linear	Linear	non-linear
3 mg/L	CM	$q_{e\ exp}$	0.1213	0.1213	0.1213	0.1213
		$q_{e\ cal}$	0.1244	0.1331	0.1392	0.1680
		k	0.0180	0.0161	0.2831	0.0961
		SSE	-	$2.76x10^{-4}$	-	$6.49x10^{-4}$
		R^2	0.9962	0.9904	0.9512	0.9834
	CMM 2%	$q_{e\ exp}$	0.1463	0.1463	0.1463	0.1463
		$q_{e\ cal}$	0.2603	0.3828	0.2352	0.6814
		k	0.0179	0.0022	0.0248	0.0018
		SSE	-	$2.72x10^{-4}$	-	$2.97x10^{-4}$
		R^2	0.7808	0.9933	0.4360	0.9931
	CMM 5%	$q_{e\ exp}$	0.1838	0.1838	0.1838	0.1838
		$q_{e\ cal}$	0.2644	0.1906	0.2055	0.2467
		k	0.0221	0.0141	0.1429	0.0542
		SSE	-	$1.34x10^{-4}$	-	$2x10^{-4}$
		R^2	0.8795	0.9975	0.9490	0.9963
5 mg/L	CM	$q_{e\ exp}$	0.1425	0.1425	0.1425	0.1425
		$q_{e\ cal}$	0.1825	0.1679	0.1774	0.2421
		K	0.0173	0.0090	0.0901	0.0282
		SSE	-	$1.56x10^{-4}$	-	$2.23x10^{-4}$
		R^2	0.9137	0.9958	0.8428	0.9939
	CMM 2%	$q_{e\ exp}$	0.1838	0.1838	0.1838	0.1838
		$q_{e\ cal}$	0.2967	0.2014	0.2352	0.2746
		K	0.0233	0.0114	0.0248	0.0351
		SSE	-	$1.47x10^{-4}$	-	$2.84x10^{-4}$
		R^2	0.9082	0.9976	0.4360	0.9952
	CMM 5%	$q_{e\ exp}$	0.2063	0.2063	0.2063	0.2063
		$q_{e\ cal}$	0.3373	0.2689	0.2645	0.4125
		K	0.0186	0.0063	0.0444	0.0106
		SSE	-	$3.75x10^{-4}$	-	$3.92x10^{-4}$
		R^2	0.7691	0.9947	0.7500	0.9945

4. Conclusion

The non-doped and mineral-doped clay-based monolith adsorbents were made, analyzed, and demonstrated effective in removing Hg^{2+} ions from water. The infrared investigations in both CM and CMM revealed the presence of identical compounds in the adsorbent, such as SiO_2, SiO-Si, OH, and Al-OH. The CMM revealed a new peak of Mn-O after manganese doping; this confirmed that the doped compounds were successfully present in the adsorbent. Morphological SEM investigation showed that manganese doping into the clay has an improved pore and site availability than pure clay monoliths. Several batch experiments were carried out, and the results showed that the contact time, adsorbent dosage, and initial concentration of Hg^{2+} solution all affected the efficiency of the adsorption process. Adsorption efficiency increased with contact duration and became steady or constant around 240 minutes. The adsorption capacity improved with a rise in adsorbate concentration due to more availability of the Hg^{2+} ions, which are attracted to the active site on the adsorbent. Maximum Hg^{2+} ions removal efficiency was observed at 42.7% after 240 minutes with an initial Hg^{2+} solution concentration of 5 mg/L and a manganese doping concentration of 5%. The highest possible efficiency values for doped manganese (CMM 2%) and non-doped manganese (CM) were 34% and 29.9%, respectively. The adsorption equilibrium data fit the Langmuir isotherm model, which had the greatest monolayer maximum adsorption capacity (Q_o) and Langmuir constant values (K_L and a_L) of 0.396 mg/g, 0.336 L/g, and 1.329 L/mg, respectively, achieved by CMM adsorbent. Based on the highest R^2 and the lowest SSE values, the pseudo-first-order non-linear adsorption kinetics model best fits the adsorption kinetics data obtained from the present study of CM and CMM. According to the findings of this investigation, CMM has a high capability for eliminating Hg^{2+} ions from water. It is necessary for future research to enhance the adsorption efficiency in removing Hg^{2+} ions from water. This effort might be made by combining clay with fillers or doping materials, such as biocarbon to increase the ability of CM and CMM to absorb Hg^{2+} ions.

Acknowledgment

The author would like to extend their gratitude to the Department of Chemical Engineering, Universitas Syiah Kuala, for providing access to the resources and facilities essential to the research completion.

References

[1] Yuncheng Wang, Tingyuan Xu, En Song, Ziquan Wang, Hu Cheng, Zhiyong Ma, Yongrong Bian, Yujie Hu, Fang Wang, Yang Song, Mercury adsorption and reduction by nonlinear optical material (NLOM) DMABR loaded on Sepiolite: A mechanism study, *Chemical Engineering Journal*, 453, (2023), 139787 https://doi.org/10.1016/j.cej.2022.139787

[2] K. Grace Pavithra, P. SundarRajan, P. Senthil Kumar, Gayathri Rangasamy, Mercury sources, contaminations, mercury cycle, detection and treatment techniques: A review, *Chemosphere*, 312, (2022), 137314 https://doi.org/10.1016/j.chemosphere.2022.137314

[3] Fengyang Wang, Shuxiao Wang, Lei Zhang, Hai Yang, Wei Gao, Qingru Wu, Jiming Hao, Mercury mass flow in iron and steel production process and its implications for mercury emission control, *Journal of Environmental Sciences*, 43, (2016), 293-301 https://doi.org/10.1016/j.jes.2015.07.019

[4] Fengyang Wang, Shuxiao Wang, Lei Zhang, Hai Yang, Qingru Wu, Jiming Hao, Characteristics of mercury cycling in the cement production process, *Journal of Hazardous Materials*, 302, (2016), 27-35 https://doi.org/10.1016/j.jhazmat.2015.09.042

[5] Krzysztof Kogut, Jerzy Gorecki, Piotr Burmistrz, Opportunities for reducing mercury emissions in the cement industry, *Journal of Cleaner Production*, 293, (2021), 126053 https://doi.org/10.1016/j.jclepro.2021.126053

[6] Qingru Wu, Shuxiao Wang, Mei Yang, Haitao Su, Guoliang Li, Yi Tang, Jiming Hao, Mercury flows in large-scale gold production and implications for Hg pollution control, *Journal of Environmental Sciences*, 68, (2018), 91-99 https://doi.org/10.1016/j.jes.2017.03.029

[7] J. Zhang, L. Han, Y. Ji, J. Wei, G. Cai, G. Gao, J. Wu, Z. Yao, Heavy metal investigation and risk assessment along the Le'An River from non-ferrous metal mining and smelting activities in Poyang, China, *Journal of Environmental Biology*, 39, 4, (2018), 536-545 https://doi.org/10.22438/jeb/39/4/MRN-681

[8] S. V. Kakareka, T. I. Kukharchyk, Trends of mercury emissions from the Chlor-Alkali industry in EECCA countries, *International Journal of Environmental Sciences*, 2, 3, (2012), 1585-1595

[9] Felix Beckers, Jörg Rinklebe, Cycling of mercury in the environment: Sources, fate, and human health implications: A review, *Critical Reviews in Environmental Science Technology*, 47, 9, (2017), 693-794 https://doi.org/10.1080/10643389.2017.1326277

[10] Janet K. Kern, Anne M. Jones, Evidence of toxicity, oxidative stress, and neuronal insult in autism, *Journal of Toxicology Environmental Health, Part B*, 9, 6, (2006), 485-499 https://doi.org/10.1080/10937400600882079

[11] Yan Zhou, Xiao-Ming Fu, Dong-Liang He, Xue-Min Zou, Cheng-Qiu Wu, Wei-Zhen Guo, Wei Feng, Evaluation of urinary metal concentrations and sperm DNA damage in infertile men from an infertility clinic, *Environmental Toxicology and Pharmacology*, 45, (2016), 68-73 https://doi.org/10.1016/j.etap.2016.05.020

[12] Penggang Pei, Yingming Xu, Lin Wang, Xuefeng Liang, Yuebing Sun, Thiol-functionalized montmorillonite prepared by one-step mechanochemical grafting and its adsorption performance for mercury and methylmercury, *Science of The Total Environment*, 806, (2022), 150510 https://doi.org/10.1016/j.scitotenv.2021.150510

[13] Ying Li, Yangxian Liu, Wei Yang, Lei Liu, Jianfeng Pan, Adsorption of elemental mercury in flue gas using biomass porous carbons modified by microwave/hydrogen peroxide, *Fuel*, 291, (2021), 120152 https://doi.org/10.1016/j.fuel.2021.120152

[14] Ke Gai, Astrid Avellan, Thomas P. Hoelen, Francisco Lopez-Linares, Evan S. Hatakeyama, Gregory V. Lowry, Impact of mercury speciation on its removal from water by activated carbon and organoclay, *Water Research*, 157, (2019), 600-609 https://doi.org/10.1016/j.watres.2019.04.006

[15] Lesley Joseph, Byung-Moon Jun, Joseph R. V. Flora, Chang Min Park, Yeomin Yoon, Removal of heavy metals from water sources in the developing world using low-cost materials: A review, *Chemosphere*, 229, (2019), 142-159 https://doi.org/10.1016/j.chemosphere.2019.04.198

[16] Adane Adugna Ayalew, Comparative adsorptive performance of adsorbents developed from kaolin clay and limestone for de-fluoridation of groundwater, *South African Journal of Chemical Engineering*, 44, (2023), 1-13 https://doi.org/10.1016/j.sajce.2022.11.002

[17] Amit Kumar Yadav, Sunipa Bhattacharyya, Preparation of porous alumina adsorbent from kaolin using acid leach method: studies on removal of fluoride toxic ions from an aqueous system, *Adsorption*, 26, (2020), 1073-1082 https://doi.org/10.1007/s10450-019-00193-4

[18] Neeraj Kumari, Chandra Mohan, Basics of clay minerals and their characteristic properties, *Clay and Clay Minerals*, 24, (2021), 1-29 https://doi.org/10.5772/intechopen.97672

[19] Mohammad Kashif Uddin, A review on the adsorption of heavy metals by clay minerals, with special focus on the past decade, *Chemical Engineering Journal*, 308, (2017), 438-462 https://doi.org/10.1016/j.cej.2016.09.029

[20] S. Meenakshi, C. Sairam Sundaram, Rugmini Sukumar, Enhanced fluoride sorption by mechanochemically activated kaolinites, *Journal of Hazardous Materials*, 153, 1-2, (2008), 164-172 https://doi.org/10.1016/j.jhazmat.2007.08.031

[21] W. M. Gitari, T. Ngulube, V. Masindi, J. R. Gumbo, Defluoridation of groundwater using Fe^{3+}-modified bentonite clay: optimization of adsorption conditions, *Desalination and Water Treatment*, 53, 6, (2015), 1578-1590 https://doi.org/10.1080/19443994.2013.855669

[22] A. Vinati, B. Mahanty, S. K. Behera, Clay and clay minerals for fluoride removal from water: a state-of-the-art review, *Applied Clay Science*, 114, (2015), 340-348 https://doi.org/10.1016/j.clay.2015.06.013

[23] Rajani Srinivasan, Advances in application of natural clay and its composites in removal of biological, organic, and inorganic contaminants from drinking water, *Advances in Materials Science and Engineering*, 2011, (2011), 872531 https://doi.org/10.1155/2011/872531

[24] G. J. Churchman, W. P. Gates, B. K. G. Theng, G. Yuan, Clays and Clay Minerals for Pollution Control, in: *Developments in Clay Science*, Elsevier, 2006, https://doi.org/10.1016/S1572-4352(05)01020-2

[25] Sadia Ata, Anila Tabassum, Ismat Bibi, Farzana Majid, Misbah Sultan, Samina Ghafoor, Muhammad Arif Bhatti, Naseem Qureshi, Munawar Iqbal, Lead remediation using smart materials. A review, *Zeitschrift für Physikalische Chemie*, 233, 10, (2019), 1377-1409 https://doi.org/10.1515/zpch-2018-1205

[26] Guodong Zhao, Huijuan Zhao, Lei Shi, Bowen Cheng, Xianlin Xu, Xupin Zhuang, In situ loading MnO_2 onto 3D Aramid nanofiber aerogel as High-Performance lead adsorbent, *Journal of Colloid Interface Science*, 600, (2021), 403-411 https://doi.org/10.1016/j.jcis.2021.05.048

[27] M. V. Miljković, Miloš Momčilović, Maja Stanković, Bratislav Ćirković, D. Laketić, Goran S. Nikolić, Maja M. Vujović, Remediation of arsenic contaminated water by a novel carboxymethyl cellulose bentonite adsorbent, *Applied Ecology and Environmental Research*, 17, 1, (2019), 733-744 http://dx.doi.org/10.15666/aeer/1701_733744

[28] M. Mylarappa, V. Venkata Lakshmi, K. R. Vishnu Mahesh, H. P. Nagaswarupa, N. Raghavendra, A facile hydrothermal recovery of nano sealed MnO_2 particle from waste batteries: An advanced material for electrochemical and environmental applications, *IOP Conference Series: Materials Science and Engineering*, 2016 https://doi.org/10.1088/1757-899X/149/1/012178

[29] S. Louati, S. Baklouti, B. Samet, Geopolymers based on phosphoric acid and illito-kaolinitic clay, *Advances in Materials Science and Engineering*, 2016, (2016), 2359759 https://doi.org/10.1155/2016/2359759

[30] Liping Kang, Menming Zhang, Zong-Huai Liu, Kenta Ooi, IR spectra of manganese oxides with either layered or tunnel structures, *Spectrochimica Acta Part A: Molecular and Biomolecular Spectroscopy*, 67, 3-4, (2007), 864-869 https://doi.org/10.1016/j.saa.2006.09.001

[31] Mohammadi Ahrouch, José M. Gatica, Khalid Draoui, Dolores Bellido, Hilario Vidal, Lead removal from aqueous solution by means of integral natural clays honeycomb monoliths, *Journal of Hazardous Materials*, 365, (2019), 519-530 https://doi.org/10.1016/j.jhazmat.2018.11.037

[32] O. W. Duckworth, N. A. Rivera, T. G. Gardner, M. Y. Andrews, C. M. Santelli, M. L. Polizzotto, Morphology, structure, and metal binding mechanisms of biogenic manganese oxides in a superfund site treatment system, *Environmental Science: Processes & Impacts*, 19, (2017), 50-58 https://doi.org/10.1039/C6EM00525J

[33] Laina Radestiani, Lia Destiarti, Winda Rahmalia, Pelapisan Mangan Dioksida pada Pasir Silika dari Kaolin Capkala dan Aplikasinya Sebagai Adsorben Besi (III) dalam Larutan, *Jurnal Kimia Khatulistiwa*, 7, 4, (2018), 8-15

[34] Yulistya Vidyaning Maulidya, Rudiyansyah Rudiyansyah, Nelly Wahyuni, Adsorpsi Senyawa Organik pada Lindi Menggunakan Cangkang Kerang Ale-Ale (*Meretrix meretrix*) Secara *Batch*, *Chimica et Natura Acta*, 9, 3, (2021), 113-117 https://doi.org/10.24198/cna.v9.n3.35607

[35] Arfiani Devi Atmasari, Faza Amaliya, Laiely Puspita Sari, Adsorption of Cr on Liquid Waste of Tannery Industry using Banana Peel Charcoal in various pH and Time Activation, *Indonesian Journal of Chemistry Environment*, 2, 1, (2019), 19-24 http://dx.doi.org/10.21831/ijce.v2i1.30292

[36] Fatemeh Gorzin, M. M. Bahri Rasht Abadi, Adsorption of Cr (VI) from aqueous solution by adsorbent prepared from paper mill sludge: Kinetics and thermodynamics studies, *Adsorption Science & Technology*, 36, 1-2, (2018), 149-169 https://doi.org/10.1177/0263617416686976

[37] Imas Eva Wijayanti, Eka Anisa Kurniawati, Solfarina Solfarina, Studi kinetika adsorpsi isoterm persamaan langmuir dan freundlich pada abu gosok sebagai adsorben, *EduChemia*, 4, 2, (2019), 175-184 http://dx.doi.org/10.30870/educhemia.v4i2.6119

[38] Darmadi, Mirna Rahmah Lubis, Munadiya Masrura, Aziz Syahfatra, Mahidin, Clay and Zeolite-Clay Based Monoliths as Adsorbents for the Hg (II) Removal from the Aqueous Solutions, *International Journal of Technology*, 14, 1, (2023), 129-141 https://doi.org/10.14716/ijtech.v14i1.5134

[39] Hui An, Bo Feng, Shi Su, Effect of monolithic structure on CO_2 adsorption performance of activated carbon fiber–phenolic resin composite: a simulation study, *Fuel*, 103, (2013), 80-86 https://doi.org/10.1016/j.fuel.2011.06.076

[40] Oscar D. Caicedo Salcedo, Diana P. Vargas, Liliana Giraldo, Juan Carlos Moreno-Piraján, Study of mercury [Hg (II)]adsorption from aqueous solution on functionalized activated carbon, *ACS Omega*, 6, 18, (2021), 11849-11856 https://doi.org/10.1021/acsomega.0c06084

[41] Zhiyuan Liu, Yong Sun, Xinrui Xu, Jingbo Qu, Bin Qu, Adsorption of Hg (II) in an aqueous solution by activated carbon prepared from rice husk using KOH activation, *ACS Omega*, 5, 45, (2020), 29231-29242 https://doi.org/10.1021/acsomega.0c03992

[42] Chenglong Zou, Jiyan Liang, Wei Jiang, Yinyan Guan, Yichen Zhang, Adsorption behavior of magnetic bentonite for removing Hg (II) from aqueous solutions, *RSC Advances*, 8, 48, (2018), 27587-27595 https://doi.org/10.1039/C8RA05247F

[43] Necmettin Caner, Ahmet Sarı, Mustafa Tüzen, Adsorption characteristics of mercury (II) ions from aqueous solution onto chitosan-coated diatomite, *Industrial Engineering Chemistry Research*, 54, 30, (2015), 7524-7533 https://doi.org/10.1021/acs.iecr.5b01293

[44] Mohammad A. Al-Ghouti, Dana Da'ana, Mohammed Abu-Dieyeh, Majeda Khraisheh, Adsorptive removal of mercury from water by adsorbents derived from date pits, *Scientific Reports*, 9, (2019), 15327 https://doi.org/10.1038/s41598-019-51594-y

[45] Dalal Z. Husein, Adsorption and removal of mercury ions from aqueous solution using raw and chemically modified Egyptian mandarin peel, *Desalination Water treatment*, 51, 34-36, (2013), 6761-6769 https://doi.org/10.1080/19443994.2013.801793

[46] Mahshid Attari, Syed Salman Bukhari, Hossein Kazemian, Sohrab Rohani, A low-cost adsorbent from coal fly ash for mercury removal from industrial wastewater, *Journal of Environmental Chemical Engineering*, 5, 1, (2017), 391-399 https://doi.org/10.1016/j.jece.2016.12.014

[47] Siti Khadijah Ab. Rahman, Nor Azah Yusof, Abdul Halim Abdullah, Faruq Mohammad, Azni Idris, Hamad A. Al-Lohedan, Evaluation of porogen factors for the preparation of ion imprinted polymer monoliths used in mercury removal, *PLoS ONE*, 13, 4, (2018), e0195546 https://doi.org/10.1371/journal.pone.0195546

[48] Risti Ragadhita, Asep Bayu Dani Nandiyanto, How to calculate adsorption isotherms of particles using two-parameter monolayer adsorption models and equations, *Indonesian Journal of Science & Technology*, 6, 1, (2021), 205-234 https://doi.org/10.17509/ijost.v6i1.32354

[49] Rama Rao Karri, J. N. Sahu, Modeling and optimization by particle swarm embedded neural network for adsorption of zinc (II) by palm kernel shell based activated carbon from aqueous environment, *Journal of Environmental Management*,

206, (2018), 178-191
https://doi.org/10.1016/j.jenvman.2017.10.026

[50] Darmadi Darmadi, Mahidin Mahidin, Siti Syifa Azzahra, Munadiya Masrura, Adsorption of mercury (II) ion in aqueous solution by using bentonite-based monolith, *Key Engineering Materials*, 885, (2021), 77-84
https://doi.org/10.4028/www.scientific.net/KEM.885.77

[51] P. C. C. Siu, Len Foong Koong, Junaid Saleem, John Barford, Gordon McKay, Equilibrium and kinetics of copper ions removal from wastewater by ion exchange, *Chinese Journal of Chemical Engineering*, 24, 1, (2016), 94-100
https://doi.org/10.1016/j.cjche.2015.06.017

[52] Pamela Becalli Vilela, Caroline Aparecida Matias, Amanda Dalalibera, Valter Antonio Becegato, Alexandre Tadeu Paulino, Polyacrylic acid-based and chitosan-based hydrogels for adsorption of cadmium: Equilibrium isotherm, kinetic and thermodynamic studies, *Journal of Environmental Chemical Engineering*, 7, 5, (2019), 103327
https://doi.org/10.1016/j.jece.2019.103327

[53] Peipeng Qiu, Shuting Wang, Chen Tian, Zhang Lin, Adsorption of low-concentration mercury in water by 3D cyclodextrin/graphene composites: synergistic effect and enhancement mechanism, *Environmental Pollution*, 252, (2019), 1133-1141
https://doi.org/10.1016/j.envpol.2019.06.034

[54] Darmadi Darmadi, Thomas S. Y. Choong, T. G. Chuah, Robiah Yunus, Y. H. Taufiq Yap, Adsorption of methylene blue from aqueous solutions on carbon coated monolith, *ASEAN Journal of Chemical Engineering*, 8, 1 & 2, (2008), 26-37

[55] Shayan Faghihi, Amin Keykhosravi, Khalil Shahbazi, Modeling of kinetic adsorption of natural surfactants on sandstone minerals: Spotlight on accurate prediction and data evaluation, *Colloid and Interface Science Communications*, 33, (2019), 100208
https://doi.org/10.1016/j.colcom.2019.100208

[56] Tauqeer Abbas, George William Kajjumba, Meena Ejjada, Sayeda Ummeh Masrura, Erica J. Marti, Eakalak Khan, Tammy L. Jones-Lepp, Recent advancements in the removal of cyanotoxins from water using conventional and modified adsorbents—A contemporary review, *Water*, 12, 10, (2020), 2756 https://doi.org/10.3390/w12102756

[57] Bibiana Karling Martini, Talita Gomes Daniel, Marcela Zanetti Corazza, Adriana Evaristo de Carvalho, Methyl orange and tartrazine yellow adsorption on activated carbon prepared from boiler residue: Kinetics, isotherms, thermodynamics studies and material characterization, *Journal of Environmental Chemical Engineering*, 6, 5, (2018), 6669-6679
https://doi.org/10.1016/j.jece.2018.10.013

[58] Yuh-Shan Ho, Review of second-order models for adsorption systems, *Journal of Hazardous Materials*, 136, 3, (2006), 681-689
https://doi.org/10.1016/j.jhazmat.2005.12.043